

pubs.acs.org/JPCC Article

Magnetic Characterization of Open-Shell Donor—Acceptor Conjugated Polymers

Daniel J. Adams, Kevin S. Mayer, Michael Steelman, and Jason D. Azoulay*



Cite This: J. Phys. Chem. C 2022, 126, 5701-5710



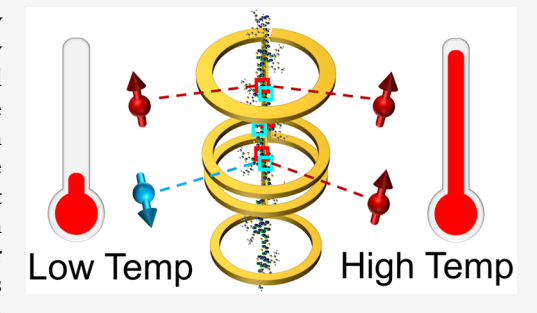
ACCESS I

Metrics & More



SI Supporting Information

ABSTRACT: Donor–acceptor (DA) conjugated polymers (CPs) with narrow bandgaps and open-shell electronic structures offer a fundamentally new paradigm for integrating the spin degree of freedom within emerging functional devices. Recent advancements have demonstrated that control of long-range electronic correlations enables low-spin (S=0) and high-spin (S=1) DA CPs, in which extended π -conjugation overcomes the intrinsic instability of these electronic configurations in light-element materials. While design strategies that articulate mechanisms of spin alignment, topology control, and quantum mechanical exchange are emerging, dedicated studies of the magnetic behavior of these materials remain rare. Here, we utilize sensitive magnetometry techniques to analyze the magnetic properties of open-shell DA CPs with low- and high-spin



ground states. We demonstrate improved measurement accuracy through combining vibrating sample magnetometry and superconducting quantum interference device magnetometry. This serves to overcome challenges associated with the inherently weak magnetic moments of these materials and a measurement environment in which the background signal is always significant and must be carefully removed. Analyzing the results following established models for paramagnetic materials enables precise quantification of the spin quantum number and temperature-dependent spin alignment. These studies articulate approaches that enable precise characterization of the bulk magnetic features of these heterogeneous and disordered materials systems, providing a path for rational property elucidation that will enable the integration of these materials within emerging technologies.

INTRODUCTION

Semiconducting donor-acceptor (DA) conjugated polymers (CPs) enable myriad opportunities for the development of devices that interact with light and transport charge. These materials form the basis for high-performance photodetectors, efficient photovoltaics, 2,3 organic field-effect transistors, 4,5 and many other emerging technologies. In open-shell organic semiconductors (OSCs) such as polycyclic aromatic hydrocarbons, ^{6,8} nanographenes, ^{9,10} graphene nanoribbons, ^{6,11,12} oligothiophenes, ¹³ and DA CPs, ^{14–18} the presence of weakly paired or unpaired electrons within the π -conjugated backbone gives rise to properties not available from their closed-shell counterparts. The capability to tailor the electronic structure and spin-spin interactions within these materials has enabled novel optical, electronic, and magnetic functionalities that can be tuned for a wide range of applications in molecular electronics, 6,19 nonlinear optics, 20 and energy conversion and storage. ^{21,22} Moreover, open-shell OSCs enable other advantageous properties that reflect their light atom composition such as weaker spin-orbit coupling and long spin lifetimes that are critical to the realization of emerging spintronic²³ and quantum technologies.²⁴

Well-defined Kekulé and non-Kekulé materials form the basis for detailed studies of open-shell materials. ^{6–8,13,24–27} These molecular systems enable connections that link chemical, electronic, and topological structures with spin—

spin coupling, exchange, physicochemical properties, and (opto)electronic functionality. 7,17,28 In contrast, the structural and energetic heterogeneities that define open-shell DA CPs complicate an articulation of how chemical, electronic, and spin structure gives rise to their properties and performance. However, these materials offer several advantages including high synthetic modularity that stems from diverse monomeric building blocks, ease of synthesis derived from the polymerization process, and unprecedented chemical stability. Furthermore, these open-shell macromolecules offer novel properties and stabilize high-spin ground states on account of their extended π -delocalization and stronger electronic correlations when compared to small molecular materials. 14 These attributes have enabled their application as highperformance conductors¹⁶ and in supercapacitors,²² thermoelectric devices, ²⁹ solution-processed infrared detectors, ³⁰ and other solid-state electronic devices. Further exploiting the spin degree of freedom within DA CPs promises completely new

Received: November 23, 2021 Revised: February 8, 2022 Published: March 22, 2022





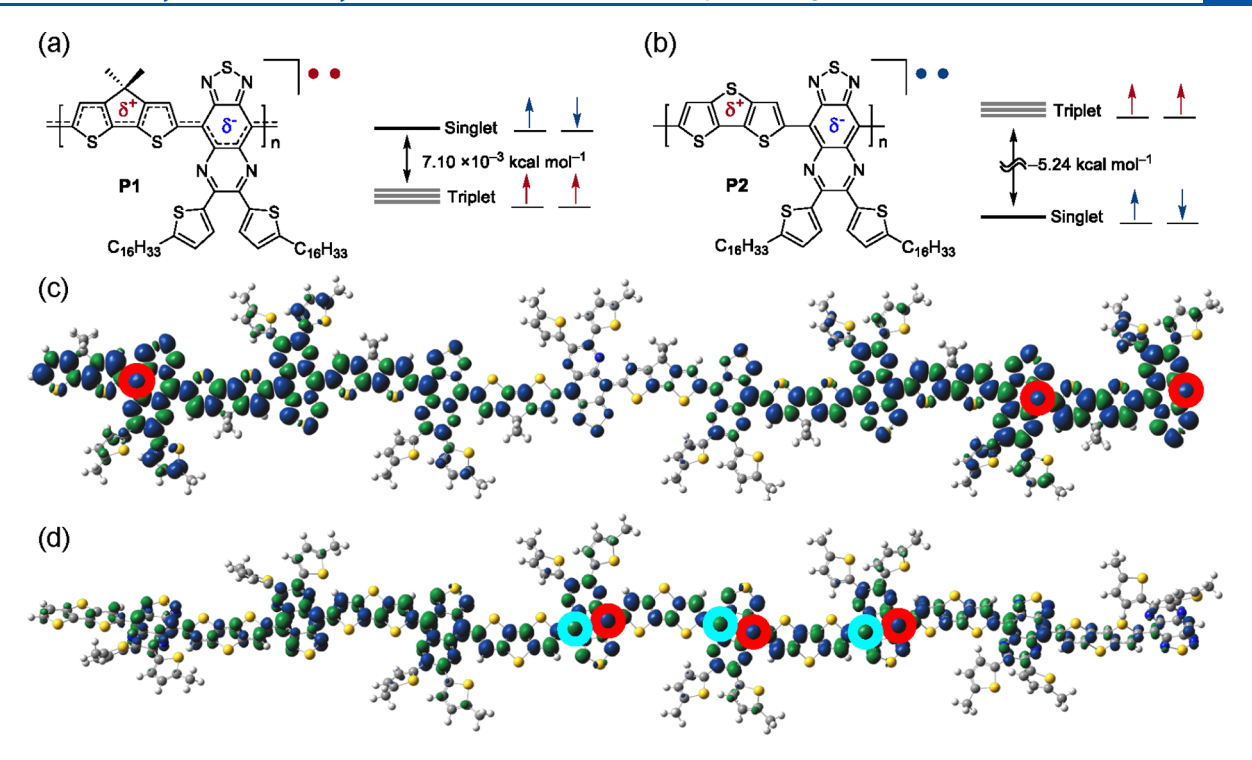


Figure 1. Molecular, electronic, and topological structure of P1 and P2. Electronic structure of high-spin P1, with a high-to-low spin energy gap $(\Delta E_{\rm ST})$ of 7.10×10^{-3} kcal mol⁻¹ and (b) P2 with a low-spin ground state and thermally populated triplet state with $\Delta E_{\rm ST}$ of -5.24 kcal mol⁻¹. (c) Spin density distribution of triplet P1 with only the most probable locations for the unpaired electrons highlighted with open circles (red: up spin). (d) Spin density distribution of singlet P2 with the most probable locations for the unpaired electrons highlighted with open circles (red: up spin and blue: down spin).

properties for these materials, which will enable their utilization within emerging (opto)electronic, spintronic, magnetic, and quantum device platforms.

It is well-established that weakly paired or unpaired spins significantly impact the properties of both inorganic and organic materials systems. 17,18,28,31 Owing to the recent development of open-shell DA CPs and their weak magnetic features and inherent disorder, reliable protocols to accurately measure and understand how magnetic properties depend on the electronic and spin structure have yet to be developed. In this class of materials, a narrowing of the bandgap gives rise to strong configurational admixing, which results in mutual repulsion of π -electrons in the highest occupied molecular orbital.³² This serves to stabilize a splitting of the electrons into nearly degenerate singly occupied molecular orbitals (SOMOs), endowing "diradical" character to the π -system. ^{13,14} This open-shell ground-state electronic configuration can be further described by the spin pairing of the two electrons relative to one another. An antiparallel (or antiferromagnetic) alignment of spins (S = 0, low spin) describes an open-shell singlet, and a parallel (or ferromagnetic) alignment of spins (S = 1, high spin) describes a triplet. Significant SOMO overlap stabilizes the singlet as the antiparallel spin alignment allows the electrons to occupy the same region of the chain. 25,33,34 However, as the bandgap is further narrowed and SOMO orthogonality increases, the triplet can drop in energy to become the ground state.

The magnetic response of open-shell CPs is largely dependent on the energy gap $(\Delta E_{\rm ST})$ between the singlet and triplet configuration. Closed-shell singlets typically possess a large $\Delta E_{\rm ST}$, leaving them with unremarkable and largely diamagnetic magnetometry signatures. However, narrow-

bandgap open-shell CPs often have a $\Delta E_{\rm ST}$ small enough to thermally populate the first spin excited state, which can be observed by measuring the moment as a function of temperature. Thus, a singlet diradical with a thermally accessible triplet excited state will have an observable diamagnetic-to-paramagnetic transition as temperature is increased and the triplet manifold is populated. In contrast, triplet diradicals have a paramagnetic signal at low temperatures. The magnetic properties are quantified by fitting to traditional equations for ideal paramagnets such as the Curie or Curie—Weiss law and Brillouin function. The modified Curie—Weiss law is defined as

$$\chi = \frac{C}{T - \theta} + \chi_0 \tag{1}$$

where χ defines the magnetic susceptibility, C is the material-dependent Curie constant, θ is the Weiss constant, and χ_0 is a vertical offset that accounts for any observable diamagnetism.

The Brillouin function for paramagnetism is

$$M = M_0 \left[\frac{2J+1}{2J} \coth \left(\frac{2J+1}{2J} \frac{gJ\mu_B H}{kT} \right) - \frac{1}{2J} \coth \left(\frac{1}{2J} \frac{gJ\mu_B H}{kT} \right) \right]$$
(2)

where M_0 is the saturation magnetization, g is the electron g-factor, $\mu_{\rm B}$ is the Bohr magneton, k is the Boltzmann constant, T is the temperature, H is the applied field, and J, the fit parameter of the Brillouin function, is the total angular momentum, which includes contributions from both the orbital and spin angular momenta, J = L + S. When $\theta = 0$,

there is no interaction between spins, and the Curie–Weiss law reduces to the original Curie law.³⁵

The copolymers considered in this study are poly(4-(4,4dimethyl-4*H*-cyclopenta[2,1-*b*:3,4-*b*']dithiophen-2-yl)-6,7-bis-(5-hexadecylthiophen-2-yl)-[1,2,5]thiadiazolo[3,4-g]quinoxaline) (P1, Figure 1a) and poly(4-(dithieno[3,2-b:2',3'd]thiophen-2-yl)-6,7-bis(5-hexadecylthiophen-2-yl)-[1,2,5]thiadiazolo[3,4-g]quinoxaline) (P2, Figure 1b). These DA CPs are composed of the same solubilizing thiadiazoloquinoxaline acceptor with ancillary hexadecylthiophene (-C₁₆H₃₃) substituents and 4,4-dimethyl-4H-cyclopenta[2,1-b:3,4-b']dithiophene (Figure 1a) or dithieno [3,2-b:2',3'-d] thiophene donors (Figure 1b). Substitution of C(CH₃)₂ at the donor bridgehead position with a S atom provides a means of controlling the bandgap and ground-state spin multiplicity.³³ As depicted in Figure 1a, P1 shows a high-spin ground state with $\Delta E_{\rm ST} = 7.10 \times 10^{-3} \text{ kcal mol}^{-1}$, while **P2** shows a lowspin ground state with $\Delta E_{\rm ST} = -5.24$ kcal mol⁻¹. In these materials, this atom-specific substitution modulates the local aromatic character within the donor, which upon extension of the π -system gives rise to dramatic differences in structural, chemical, electronic, and spin-pairing properties of the polymers.³³ Figure 1c,d shows the spin-density distribution of n = 8 oligomers modeled using density functional theory calculations at the unrestricted (U)B3LYP/6-31G** level of theory for P1 and P2, respectively. 36,37 For the singlet diradical, there is significant overlap between α - and β -SOMOs, whereas the triplet minimizes the overlap, with spins occupying separate spaces. Thus, the topological structures of P1 (Figure 1c) and P2 (Figure 1d) manifest from long-range π -interactions along the conjugated backbone, which facilitates control between low-spin aromatic and high-spin quinoidal forms. These materials represent some of the first examples of open-shell DA CPs with different spin states that enable the opportunity for careful and comparative studies of the magnetic properties.

Here, we report the results of the sensitive magnetic characterization of P1 and P2 using superconducting quantum interference device (SQUID) magnetometry. While continuous-wave (CW) and pulsed electron paramagnetic resonance (EPR) spectroscopy provide a wealth of information about materials with unpaired electrons and their spin dynamics and electronic structure, direct-current (DC) magnetometry provides information that is not available using EPR. This includes the bulk magnetic response, including temperaturedependent majority spin alignment, magnetic phase transitions, diamagnetic susceptibility, morphological dependencies, and their relative contribution to the magnetic features. These observables are fundamentally and critically important in the study of emerging semiconductor devices. Thus, we characterize the ground-state behavior and thermal activation of the spin transitions through temperature-dependent measurements from 2 to 400 K. Through these studies, we overcome difficulties in accurately measuring small magnetic moments with comparatively large background signals such as those that are ubiquitous in open-shell diradicals. We further enhance the measurement sensitivity by utilizing vibrating sample magnetometry (VSM) and critically compare and contrast the VSM and standard DC measurement modes for weakly magnetic organic material systems.

RESULTS AND DISCUSSION

Magnetic Characterization of Open-Shell CPs. Measurements reported here were carried out using the MPMS3 from Quantum Design. While SQUID magnetometry presents a robust and sensitive means of detecting small magnetic fields of weakly magnetic samples on the order of 5×10^{-8} emu, combining this technique with VSM enhances the sensitivity at least 5-fold to less than 1×10^{-8} emu (Figure S1). This produces higher-quality data for small magnetic moments. While commonly used to measure magnetic properties of inorganic materials, this technique has also been applied to carbon thin films,³⁸ nanofibers,³⁹ and nanotubes⁴⁰ and offers significant utility when measuring these low-moment materials. The nature of the sample holder must also be considered as this can be a major contributor to the background signal and can dramatically overshadow signals that arise from weak magnetic moments. While VSM offers greater sensitivity, the DC scan offers more versatility in the choice of the sample holder. Thus, straws are widely utilized due to their low intrinsic magnetic moment; however, defect-induced magnetic responses can occur from bending or creasing (Figure S2). While numerous reports review limits and considerations concerning these techniques, these typically detail the measurement and detection of coercivity or apparent coercivity in inorganic materials. 41-43 However, detailed magnetic studies and procedures for measurements of low-moment OSC materials have not been clearly articulated for open-shell organic diradicals.

We begin by measuring P1 using the DC scan mode (or DC scan). As shown in Figure 2, the sample was packed in a

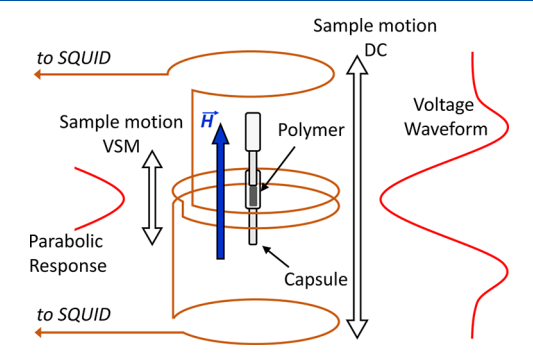


Figure 2. Schematic depiction of magnetometry measurement of a DA CP sample within a powder sample capsule (sample holder not shown). The sample traverses through the gradiometer, which is coupled to the SQUID. In the DC mode (right), the sample moves through the length of the gradiometer, producing a voltage waveform in response to an applied magnetic field **H**. In the VSM mode (left), the sample oscillates within a much smaller region of the gradiometer, producing a simpler response.

powder sample holder from Quantum Design, which was fixed within the brass half-tube sample holder. Figure 2 shows the measurement diagram for the DC scan and the path the sample travels through the gradiometer, inducing a voltage as it moves. This is related to its magnetization by the applied field H and is recorded as a function of the sample position. This voltage is output as a magnetic signal by fitting to a voltage waveform

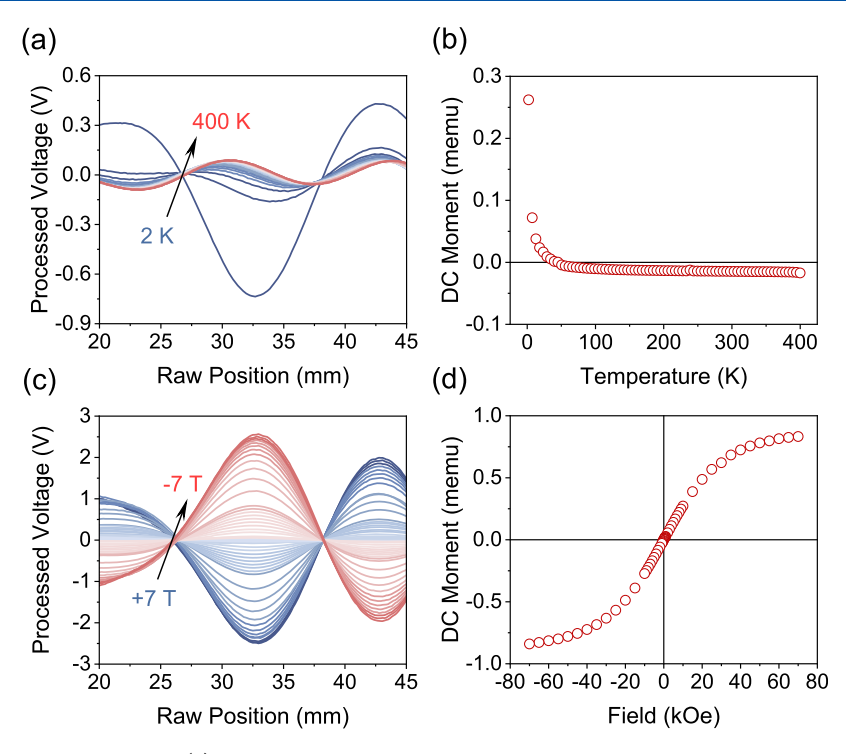


Figure 3. Field-dependent DC scans of **P1.** (a) Processed voltage versus raw sample position within the MPMS3 gradiometer with varying temperature and a constant magnetic field H of 1 T. (b) Magnetic moment versus T, generated automatically from voltage measurements shown in part (a). (c) Processed voltage versus raw sample position with a varying magnetic field and a constant temperature of 2 K (d) Magnetic moment versus H, generated automatically from voltage measurements shown in part (b).

$$V(z) = S + A(2[R^{2} + (x - C)^{2}]^{-3/2}$$

$$- [R^{2} + (L + x - C)^{2}]^{-3/2}$$

$$- [R^{2} + (-L + x - C)^{2}]^{-3/2})$$
(3)

where S is an offset, A is the amplitude, C is the center position, R is the gradiometer radius, L is the length, and the raw position x is the independent variable.

The temperature dependence of the magnetic moment was recorded for P1 in a constant magnetic field of 1 T from 2 to 400 K. Figure 3a shows the processed voltage signal as a function of the sample position within the gradiometer, while Figure 3b shows the associated magnetic moment. The largest voltage amplitude in Figure 3a corresponds to the 2 K measurement, which has the largest magnetic moment. As the temperature is increased, the magnetic moment decreases rapidly, following a Curie-like trend. This sharp reduction in the magnetic moment is observed in the MPMS3 output in Figure 3b. Following this, the field dependence of the magnetic moment was measured in the DC mode for $-7 \le H \le 7$ T at a constant temperature of 2 K. Figure 3c shows the position dependence of the processed voltage, and the associated magnetic moment output is shown in Figure 3d.

A difficulty of DC scans arises when the sample holder assembly represents a significant part of the measured magnetic signal, as this will affect the shape of the voltage versus position curve. In the DC scan of P1, the background is significant, and this is reflected in Figure 3a,c, where one local maximum was found to be as high as 80% of the absolute maximum. It is well-established that background subtraction is not straightforward for the DC scan, and improper handling can significantly impact the reported moment. Point-by-point background subtraction is not valid for DC measurements.

Thus, manual background subtraction was accomplished by subtracting the processed voltage of the background from that of original data and fitting the result to the voltage waveform of eq 3, where S, A, and C are the fitting parameters and R and L are fixed. The amplitude is then multiplied by the calibration factor, specific to each system and determined using a Pd standard. This factor relates the voltage amplitude to the magnetic moment. If the voltage waveform function fails to properly fit the measured waveform, then the reported magnetic moment is unreliable.

In contrast, VSM measurements offer enhanced sensitivity and a lower noise floor (Figure S1), with differences in magnetic moment detection between the two measurement modes of approximately 0.5 μ emu. Rather than traversing the length of the gradiometer coil, as in the DC scan, the sample is vibrated at a set amplitude in the center of the coil (Figure 2), allowing for the utilization of only a small portion of the voltage waveform. Noise is largely reduced due to the frequency-dependent voltage variation differing from the mechanical frequency, which is beneficial for low-moment samples (on the order of 10^{-7} emu). Background subtractions are significantly less involved and are accomplished using a simple point-by-point subtraction.

Characterization of Temperature-Dependent Susceptibility. The temperature-dependent magnetic susceptibility (χ) has been widely used to determine the magnetic phase and thermally induced changes. ^{16,45} In the case of openshell diradicals, a magnetic transition may appear, indicating a change in the majority electron spin alignment. ⁴⁶ Recently, this type of measurement was applied to CPs to study the delocalization of polarons through analysis of both Curie and temperature-independent Pauli paramagnetism and draw relationships between magnetic properties and conductiv-

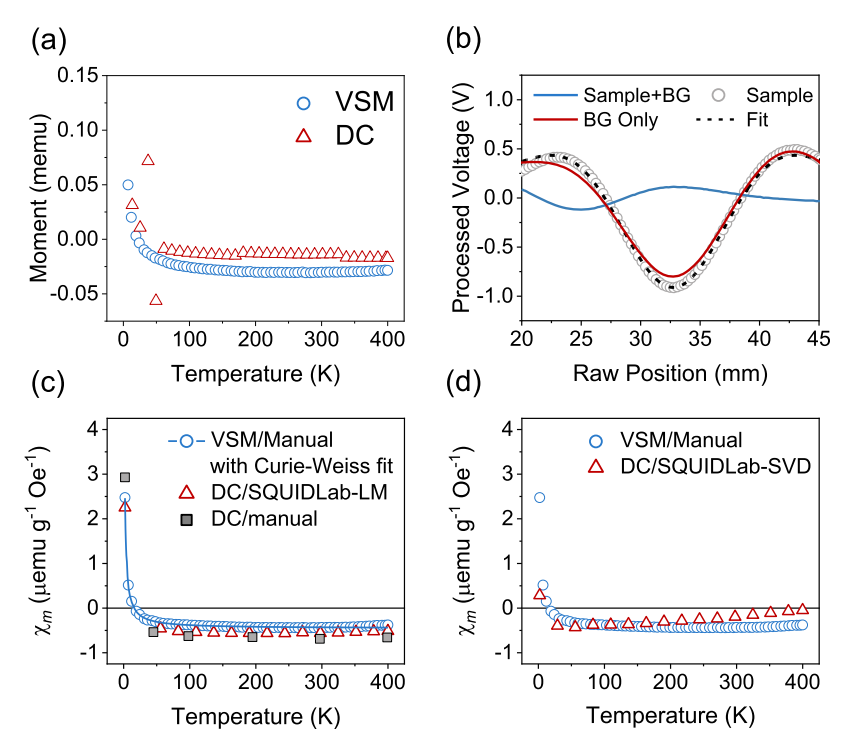


Figure 4. Temperature-dependent magnetic characterization of P1. (a) Magnetic moment versus T measured via DC and VSM scans. (b) Measured sample, background, and subtracted voltage waveforms fit to the voltage waveform of eq 3 at 2 K. (c) Mass susceptibility $\chi_{\rm m}$ versus T for VSM and DC measurements after point-by-point VSM, manual DC, and SquidLab LM-fit background subtractions, with the Curie—Weiss fit to the VSM data. (d) Mass susceptibility $\chi_{\rm m}$ versus T for VSM and DC measurements after point-by-point VSM, manual DC, and SquidLab SVD-fit background subtractions.

ity. 47,48 The magnetic moment of P1 was recorded as a function of temperature from 2 to 400 K with a field of 1 T in both the VSM and DC measurement modes. Figure 4a shows the measured magnetic moment for both detection modes, with clear differences between the two uncorrected measurements. For the VSM measurement, point-by-point subtraction was utilized to obtain the sample magnetic moment, which was then converted to mass susceptibility (χ_m) . The range of χ_m was found to be on the order of 10^{-6} emu/g Oe over the entire temperature range, from 2 to 400 K, with $\chi_{\rm m}$ trending around 5 \times 10⁻⁷ emu/g Oe from approximately 50–400 K. In the DC scan, manual background subtraction was performed first by subtracting the background waveform from the sample waveform and applying eq 3 along with the calibration factor to determine the magnetic moment. Figure 4b shows an example of the initial, background, and subtracted waveforms at 2 K, with the subtracted waveform fitted to eq 3, which is necessary for manual determination of the magnetic moment. A comparison of these background subtractions is shown in Figure 4c, where the two measurement modes are found to be in closer agreement after this correction.

An automated DC background subtraction was also performed for comparison using SquidLab, ⁴⁹ which offers options for signal processing and dipole fitting algorithms, with both options attempted here (Figure 4c,d). Before attempting the background subtraction and fitting, the smoothing option was used on the raw background data, which was found to be noisy. After performing the automated background subtraction, the Levenberg—Marquardt (LM)^{50,51} dipole-fitting option was selected. This is the same algorithm implemented by the MPMS3 for dipole fitting and is widely used for curve fitting. The routine begins with parameter initialization, with high

accuracy possible with appropriate initial values.⁵² The result of the background subtraction and LM fitting option for P1 is included in Figure 4c and is also found to be in agreement with the VSM result. A second automated fitting was attempted on the data following background subtraction using a singular value decomposition (SVD),53 which does not rely on an estimate of starting points and is reported to extract useable dipole forms from noisy data or weak signals with high accuracy. 49 Figure 4d shows a comparison of the backgroundsubtracted χ determined through VSM data to the susceptibility determined from the automated SVD fitting to the waveforms. Although the form of the temperature-dependent signal is consistent in the 2-50 K range, the susceptibilities quickly diverge, with a trendline forming in the SVD-fit data that was not observed in the other three analyses of the temperature-dependent susceptibility of P1. The upward trend indicates that $\chi_{\rm m}$ increases from -0.4 to 0 μ emu/g Oe, which would imply a thermal population of a triplet state. This gives the erroneous appearance of approaching a paramagnetic phase within the measured temperature range.

P1 is paramagnetic in the ground state, with an apparent diamagnetic transition occurring at 17 K. A fit of the P1 VSM data to the Curie—Weiss law (eq 1) is shown in Figure 4c. The fit gives a small Weiss constant of $\theta = -0.5$ K. This indicates weak, short-range antiferromagnetic interactions among populations of nearest-neighbor spins. A small but clear difference is observed between fitting with $\theta = 0$ and $\theta = -0.5$ K (Figure S3), indicating that the low-temperature behavior of P1 differs from that of a classical paramagnet, in which spins are completely noninteracting. Interactions between local moments in P1 serve to reduce the overall χ at the lowest temperatures, as indicated by the negative Weiss constant, ³⁵

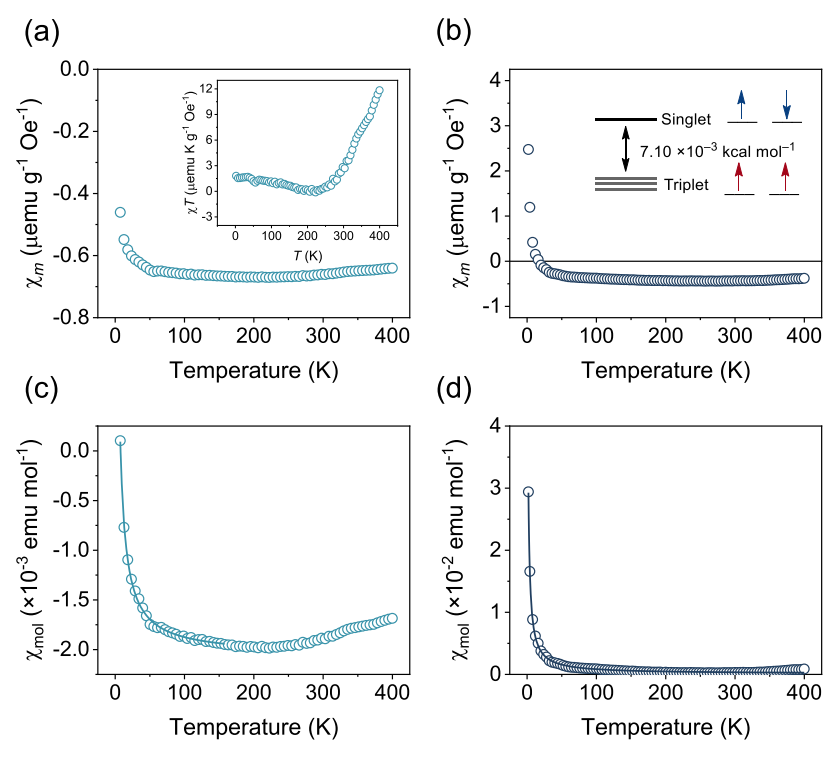


Figure 5. Temperature-dependent magnetic properties of P1 and P2. (a) Mass susceptibility, χ_{m} , versus T from 2 to 400 K of P2. Inset: Observed $\chi_m T$ versus T dependence. (b) χ_m versus T from 2 to 400 K of P1, with associated ΔE_{ST} . (c) Molar susceptibility (χ_{mol}) versus T from 2 to 400 K of P2, with the Curie-like region fit to the Curie-Weiss law (eq 1). The divergence from the Curie-like behavior with increased temperature is apparent with the smaller scale of the χ_{mol} axis. (d) χ_{mol} versus T from 2 to 400 K of P1, with fitting to the Curie-Weiss law.

while spin-spin interactions are less important at higher temperatures.

When performing a background subtraction, regardless of the measurement mode, there are several considerations to keep in mind.44 First, it is important to run the original and background measurements using the same sequence and allowing the system to stabilize at each field or temperature point in which the magnetic moment will be recorded, both to ensure consistency between the sample and background measurements and to ensure the equilibrium between the sample and environment during the measurement. It is also recommended to make sure that the sample rod is in the same rotational position for each measurement to ensure that there will be no radial offset between the two measurements. Finally, it is necessary to ensure consistency between the sample holder for the original measurement and the background. This includes checking the size of the capsule chosen to hold the sample. In the case of the brass sample holder and VSM capsule, a gap must be left between the top and bottom capsule pieces that is equal to the size of the sample space. The easiest way to do this is to measure the total length of the capsule using a caliper (Figure S4). Note that, in the case of the DC scan, the raw data file must also be saved, which is not saved by default.

SQUID-VSM was used to measure the magnetic moment of P2 over the same temperature range with H=1 T. Figure 5a shows the temperature-dependent $\chi_{\rm m}$ after a background correction, where there are several notable features. The first is that $\chi_{\rm m}$ is negative over the whole temperature range, including the low-temperature region, where there is an upturn following a general Curie-like trend, which indicates that diamagnetic behavior is dominant in this sample. Another feature is the thermal enhancement of the paramagnetic moment indicated

by a sharp upturn in $\chi_{\rm m}$, diverging from the typical Curie-like behavior starting from approximately 200 K. This represents the beginning of the thermal population of the triplet state and is distinct from P1 (Figure 5b), which has a positive lowtemperature χ_m that levels off as temperature is increased, with no enhancement at high temperatures. To properly identify the upturn as a thermal population of the paramagnetic state, care must be taken when handling the data to ensure that this is not an artifact of the background subtraction. For example, measurements of certain sample holders, particularly the brass half-tube with a blank VSM capsule, may tend to have a magnetic moment that trends significantly toward negative values in the high-temperature range, usually beginning around room temperature (Figure S5). For sample moments on the order of 10^{-6} emu, as is the case for our samples (Figure 4c), this downward trend between 300 and 400 K is often observed in the measurement of the sample as well, and the subtraction offsets this trend. Here, the upturn begins around 200 K and is found to be reproducible across sample batches and measurement modes.³³ The upward trend is the clearest in the representation of $\chi_m T$ versus T shown in Figure 5a after correcting for the diamagnetic moment. The magnitude of $\chi_{\rm m}$ of P2 is an order of magnitude smaller than that of P1, consistent with weak diamagnetism of the singlet state.

In many materials, the weak intrinsic diamagnetism is essentially negligible relative to other magnetic phases present and can often be disregarded. However, in low-moment organic materials with unpaired electrons, the diamagnetic contribution is often observable or even dominant. The intrinsic diamagnetism of these materials can be accounted for using Pascal's constants, diamagnetic correction factors tabulated from a collection of previous studies⁵⁴ that provide a net diamagnetic correction factor to the susceptibility in

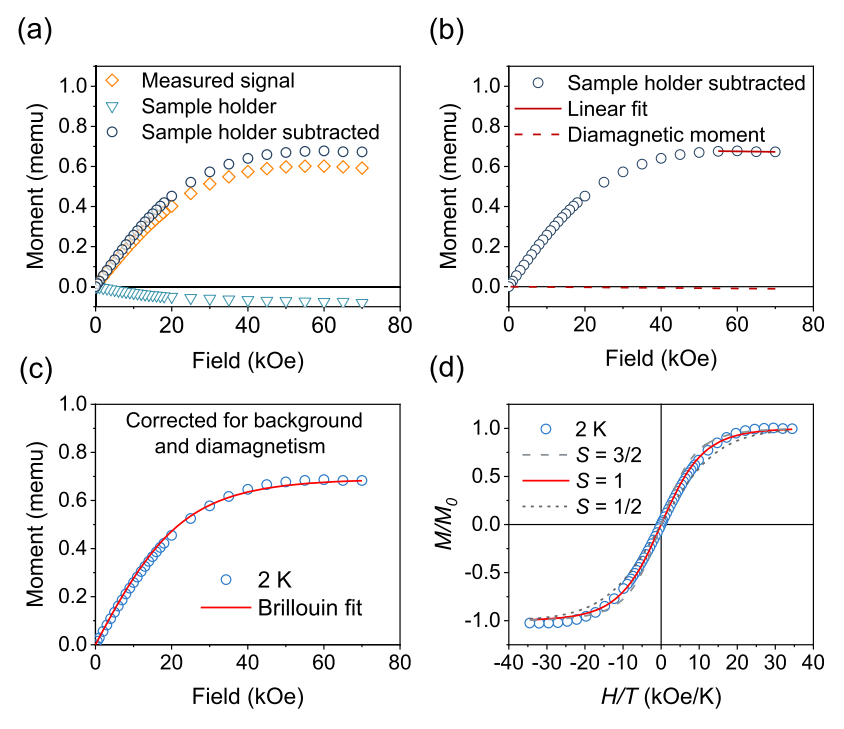


Figure 6. Field-dependent magnetic moment isotherms at 2 K for P1. (a) Magnetic moment versus H compared to the magnetic background contribution of the brass sample holder. (b) Background-subtracted magnetic moment with a linear fit to the high-field portion of the curve to calculate the field-dependent diamagnetic moment. (c) Magnetic moment versus H corrected for both background and diamagnetism, fit to the paramagnetic Brillouin function (eq 2) to show a high-spin ground state. (d) Normalized magnetization versus H/T of P1 over the full field range, $T \le H \le -7$ T, with multiple spin values compared. The best representation of the data is achieved with S = 1.

order to theoretically remove the intrinsic diamagnetic contribution.

Pascal's corrections were applied to the data for P1 and P2 to correct for diamagnetism of the individual components. This strategy is broadly applied to small-molecule materials⁵⁴ and was compared to the CPs here to understand the utility and validity of this approach for removal of the intrinsic diamagnetic susceptibility from these macromolecular materials systems. We note, however, that these corrections were previously applied to materials with well-defined electronic structures and that our materials possess highly delocalized wavefunctions. 55,56 Thus, their chemical constituents may exist in more hybridized electronic configurations, between aromatic and quinoidal forms, with variations in the topological location of spin density along the polymer chain. Furthermore, P1 and P2 are composed of macromolecules of different sizes, defined by the dispersity (D) of the sample. These attributes may contribute to and alter the actual susceptibility and complicate the diamagnetic correction.5

To apply these constants, which are reported in emu/mol, the data must be converted to molar susceptibility ($\chi_{\rm mol}$). In the linear region of paramagnetic magnetization, χ is approximately field-independent. The assumption of field independence at the measurement field of 1 T is then valid in this case, and the correction factor based on Pascal's constants can be applied to the $\chi_{\rm mol}$ versus T data. When comparing the data using Pascal's corrections to uncorrected data, the diamagnetic susceptibility of P2 is reduced but not eliminated (Figure 5c). In contrast, P1 is found to follow a Curie–Weiss trend with a negligible vertical offset χ_0 (Figure 5d). This differs from the diamagnetic transition previously observed at low temperature, which was dominant over the majority of the temperature range, from 100 to 400 K (Figure 5d).

The variation in χ_{mol} of **P2** over the entire temperature range is 0.002 emu/mol, an order of magnitude smaller than that of **P1**, which has a variation of 0.03 emu/mol. Fitting χ_{mol} versus T for **P2** to eq 1 (Figure 5c) in the Curie-like region before the upturn gives a Curie constant of 0.018 emu/mol, only 24% of that of **P1**, which had a Curie constant 0.074 emu/mol. Thus, **P1** will have larger χ over the temperature range. The fit also gives $\theta = -1.3$ K for **P2**, implying that the low-temperature antiferromagnetic interactions are more significant in **P2** than in **P1**. These results suggest a more complicated diamagnetic contribution to both **P1** and **P2** than can be calculated from closed-shell components alone, which likely emanates from the macromolecular nature of these materials.

Determination of the Ground-State Spin Quantum **Number.** An important figure of merit for characterizing open-shell conjugated materials with the potential for a highspin ground state is the spin quantum number. The spin quantum number can be evaluated by measuring the fielddependent magnetization isotherm, where the lowest temperature available is used for characterizing the ground state.⁵⁹ SQUID-VSM was used to measure the magnetization versus field for P1 as well as for the sample holder in order to perform a background subtraction (Figure 6a). A common, though sometimes subtle, feature of the magnetization curve in dilute spin samples is the prevalence of the diamagnetic contribution at high magnetic fields, 42 when the paramagnetic phase is saturated and therefore unchanged. A linear fit to the negativeslope portion of the magnetization versus field curve allows for the modeling and subtraction of the diamagnetic contribution, 60 as shown in Figure 6b. This is particularly important for quantifying the spin quantum number in organic diradicals, where the paramagnetic moment of the conjugated backbone is weak, and the intrinsic diamagnetic moment due to closedshell components, such as solubilizing long alkyl chain additions that enable practical processing methods, impacts the shape of the curve.

It is important to note that the magnetic field of the MPMS is supplied using a superconducting coil, a niobium-titanium solenoid, with a transition temperature of around 10 K. The coil temperature is independent of the measurement temperature, allowing for the coil to be perpetually maintained in a superconducting state. The advantage of using a superconducting coil is that once charged, the current will persist indefinitely, as long as the coil remains in a superconducting state. Thus, the current of the power supply can be ramped to zero while the magnet remains charged. A standard problem encountered with the use of a superconducting coil is the occurrence of remanence, manifesting as an offset or a field error. At first inspection, the residual field offset can create the illusion of coercivity. However, for a magnetically reversible material, or a sample with a small hysteresis, the hysteresis is inverted. This effect can be accounted for by measuring a pure paramagnetic sample of known mass and susceptibility, such as a Pd standard, as a field correction sample. The measured moment can then be converted to a true field (Figure S6).⁶¹

Significant remanence can be introduced from set fields of around 1000 Oe, 62 so it is important to perform the field correction on any measurement from above or near this field value. Since the superconducting coil is always kept at the same temperature, regardless of the measurement temperature, the observed remanence is temperature-independent. The amount of remanence is specific to each coil, so there are no standard field correction values, and the corrected fields must be determined for each instrument and measurement. It is also dependent on the charging history of the magnet, including field magnitude, direction, and ramp rate, so the field correction sample must be run using the same measurement sequence for field values and ramp rates. Remanence can be reduced by returning the field to zero in oscillate mode from a field greater than 1 T. In this mode, the controller will overshoot the target field by 70% of the field change. If the target field is zero, this mode gives the nearest true value of 0 Oe.º

After correcting for the background, diamagnetic contribution, and field offset, the resultant moment is the paramagnetic contribution of the unpaired electrons in the diradical sample. The spin quantum number was then determined using the Brillouin function (eq 2). An often valid assumption in the case of solid materials is the quenching of the orbital moment.³⁵ EPR studies of P1 give a sharp Lorentzian line shape centered around g = 2.0039 (see Figure 5a in ref 33). The Landé equation ⁶³ gives a g-factor of 2 when L = 0 and J = S, which supports this assumption and allows for the substitution of J =S in the Brillouin function. Fitting the magnetometry result for P1 at the lowest temperature after correcting for the remanent field gives S = 0.92, consistent with a triplet ground state (Figure 6c). Figure 6d shows the measurement over the full sweep range, $7 \le H \le -7$ T, after background and diamagnetic correction and normalized to the saturation magnetization M_0 . For comparison, the Brillouin function with S = 1/2, 1, and 3/ 2 is shown, with the best representation of the data achieved with S = 1.

CONCLUSIONS

CPs with controlled diradical character represent an important class of materials for a variety of emerging applications.

Sensitive magnetometry measurements of two structurally related but electronically distinct DA CPs were carried out using different measurement modes, and the useable signals were carefully extracted by separating them from extrinsic and less relevant contributions. Experimental techniques and characterization paradigms were reviewed for their merit, and detailed procedures for handling data and applying models were covered. As the spin properties are thought to impact physical properties and (opto)electronic functionality in this class of materials, accurate determination of the spin properties will lead the way to new technologies based on open-shell OSCs. The copolymers studied here reveal a shift form a lowspin structure with thermal activation of the paramagnetic moments in P2 to a high-spin structure with robust lowtemperature spin properties in P1, which give near-perfect fits to the model functions for an ideal paramagnet. χ_{mol} for P2 showed a much smaller Curie constant and a larger θ than P1, which indicate weaker susceptibility and stronger antiferromagnetic interactions, respectively. These results are consistent with a triplet ground state for P1 and a singlet ground state for P2.

ASSOCIATED CONTENT

Supporting Information

The Supporting Information is available free of charge at https://pubs.acs.org/doi/10.1021/acs.jpcc.1c10020.

Additional experimental details and methods, including additional plots, background measurements, and a photograph of the sample preparation (PDF)

AUTHOR INFORMATION

Corresponding Author

Jason D. Azoulay — Center for Optoelectronic Materials and Devices, School of Polymer Science and Engineering, The University of Southern Mississippi, Hattiesburg, Mississippi 39406, United States; Orcid.org/0000-0003-0138-5961; Email: jason.azoulay@usm.edu

Author

Daniel J. Adams — Center for Optoelectronic Materials and Devices, School of Polymer Science and Engineering, The University of Southern Mississippi, Hattiesburg, Mississippi 39406, United States

Kevin S. Mayer — Center for Optoelectronic Materials and Devices, School of Polymer Science and Engineering, The University of Southern Mississippi, Hattiesburg, Mississippi 39406, United States

Michael Steelman — Center for Optoelectronic Materials and Devices, School of Polymer Science and Engineering, The University of Southern Mississippi, Hattiesburg, Mississippi 39406, United States

Complete contact information is available at: https://pubs.acs.org/10.1021/acs.jpcc.1c10020

Author Contributions

The manuscript was written through contributions of all authors. All authors have given approval to the final version of the manuscript.

Notes

The authors declare no competing financial interest.

ACKNOWLEDGMENTS

The work performed at The University of Southern Mississippi was made possible through the National Science Foundation (OIA-1757220) and the Air Force Office of Scientific Research (AFOSR) under support provided by the Organic Materials Chemistry Program (Grant FA9550-20-1-0353, Program Manager: Dr. Kenneth Caster).

REFERENCES

- (1) Li, N.; Mahalingavelar, P.; Vella, J. H.; Leem, D.-S.; Azoulay, J. D.; Ng, T. N. Solution-Processable Infrared Photodetectors: Materials, Device Physics, and Applications. *Mater. Sci. Eng., R* **2021**, *146*, 100643.
- (2) Holliday, S.; Li, Y.; Luscombe, C. K. Recent Advances in High Performance Donor-Acceptor Polymers for Organic Photovoltaics. *Prog. Polym. Sci.* **2017**, *70*, 34–51.
- (3) Armin, A.; Li, W.; Sandberg, O. J.; Xiao, Z.; Ding, L.; Nelson, J.; Neher, D.; Vandewal, K.; Shoaee, S.; Wang, T.; et al. A History and Perspective of Non-Fullerene Electron Acceptors for Organic Solar Cells. *Adv. Energy Mater.* **2021**, *11*, 2003570.
- (4) Wang, C.; Dong, H.; Hu, W.; Liu, Y.; Zhu, D. Semiconducting π -Conjugated Systems in Field-Effect Transistors: A Material Odyssey of Organic Electronics. *Chem. Rev.* **2012**, *112*, 2208–2267.
- (5) Kim, M.; Ryu, S. U.; Park, S. A.; Choi, K.; Kim, T.; Chung, D.; Park, T. Donor—Acceptor-Conjugated Polymer for High-Performance Organic Field-Effect Transistors: A Progress Report. *Adv. Funct. Mater.* **2020**, *30*, 1904545.
- (6) Gopalakrishna, T. Y.; Zeng, W.; Lu, X.; Wu, J. From Open-Shell Singlet Diradicaloids to Polyradicaloids. *Chem. Commun.* **2018**, *54*, 2186–2199.
- (7) Sun, Z.; Ye, Q.; Chi, C.; Wu, J. Low Band Gap Polycyclic Hydrocarbons: From Closed-Shell Near Infrared Dyes and Semiconductors to Open-Shell Radicals. *Chem. Soc. Rev.* **2012**, *41*, 7857–7889.
- (8) Sun, Z.; Zeng, Z.; Wu, J. Zethrenes, Extended p-Quinodimethanes, and Periacenes with a Singlet Biradical Ground State. *Acc. Chem. Res.* **2014**, *47*, 2582–2591.
- (9) Song, S.; Su, J.; Telychko, M.; Li, J.; Li, G.; Li, Y.; Su, C.; Wu, J.; Lu, J. On-Surface Synthesis of Graphene Nanostructures with π -Magnetism. *Chem. Soc. Rev.* **2021**, *50*, 3238–3262.
- (10) Morita, Y.; Suzuki, S.; Sato, K.; Takui, T. Synthetic Organic Spin Chemistry for Structurally Well-Defined Open-Shell Graphene Fragments. *Nat. Chem.* **2011**, *3*, 197–204.
- (11) Magda, G. Z.; Jin, X.; Hagymási, I.; Vancsó, P.; Osváth, Z.; Nemes-Incze, P.; Hwang, C.; Biró, L. P.; Tapasztó, L. Room-Temperature Magnetic Order on Zigzag Edges of Narrow Graphene Nanoribbons. *Nature* **2014**, *514*, 608–611.
- (12) Ruffieux, P.; Wang, S.; Yang, B.; Sánchez-Sánchez, C.; Liu, J.; Dienel, T.; Talirz, L.; Shinde, P.; Pignedoli, C. A.; Passerone, D.; et al. On-Surface Synthesis of Graphene Nanoribbons with Zigzag Edge Topology. *Nature* **2016**, *531*, 489–492.
- (13) Casado, J.; Ponce Ortiz, R.; López Navarrete, J. T. Quinoidal Oligothiophenes: New Properties Behind an Unconventional Electronic Structure. *Chem. Soc. Rev.* **2012**, *41*, 5672–5686.
- (14) London, A. E.; Chen, H.; Sabuj, M. A.; Tropp, J.; Saghayezhian, M.; Eedugurala, N.; Zhang, B. A.; Liu, Y.; Gu, X.; Wong, B. M.; et al. A High-Spin Ground-State Donor-Acceptor Conjugated Polymer. *Sci. Adv.* 2019, 5, No. eaav2336.
- (15) Yuen, J. D.; Wang, M.; Fan, J.; Sheberla, D.; Kemei, M.; Banerji, N.; Scarongella, M.; Valouch, S.; Pho, T.; Kumar, R.; et al. Importance of Unpaired Electrons in Organic Electronics. *J. Polym. Sci., Part A: Gen. Pap.* **2015**, *53*, 287–293.
- (16) Huang, L.; Eedugurala, N.; Benasco, A.; Zhang, S.; Mayer, K. S.; Adams, D. J.; Fowler, B.; Lockart, M. M.; Saghayezhian, M.; Tahir, H.; et al. Open-Shell Donor—Acceptor Conjugated Polymers with High Electrical Conductivity. *Adv. Funct. Mater.* **2020**, *30*, 1909805.

- (17) Chen, Z. X.; Li, Y.; Huang, F. Persistent and Stable Organic Radicals: Design, Synthesis, and Applications. *Chem* **2021**, *7*, 288–332.
- (18) Ji, X.; Fang, L. Quinoidal Conjugated Polymers with Open-Shell Character. *Polym. Chem.* **2021**, *12*, 1347–1361.
- (19) Huang, Y.; Egap, E. Open-Shell Organic Semiconductors: An Emerging Class of Materials with Novel Properties. *Polym. J.* **2018**, *50*, 603–614.
- (20) Nakano, M. Open-Shell-Character-Based Molecular Design Principles: Applications to Nonlinear Optics and Singlet Fission. *Chem. Rec.* **2017**, *17*, 27–62.
- (21) Morita, Y.; Nishida, S.; Murata, T.; Moriguchi, M.; Ueda, A.; Satoh, M.; Arifuku, K.; Sato, K.; Takui, T. Organic Tailored Batteries Materials Using Stable Open-Shell Molecules with Degenerate Frontier Orbitals. *Nat. Mater.* **2011**, *10*, 947–951.
- (22) Wang, K.; Huang, L.; Eedugurala, N.; Zhang, S.; Sabuj, M. A.; Rai, N.; Gu, X.; Azoulay, J. D.; Ng, T. N. Wide Potential Window Supercapacitors Using Open-Shell Donor—Acceptor Conjugated Polymers with Stable N-Doped States. *Adv. Energy Mater.* **2019**, *9*, 1902806.
- (23) Li, D.; Yu, G. Innovation of Materials, Devices, and Functionalized Interfaces in Organic Spintronics. *Adv. Funct. Mater.* **2021**, *31*, 2100550.
- (24) Lombardi, F.; Lodi, A.; Ma, J.; Liu, J.; Slota, M.; Narita, A.; Myers, W. K.; Müllen, K.; Feng, X.; Bogani, L. Quantum Units from the Topological Engineering of Molecular Graphenoids. *Science* **2019**, 366, 1107–1110.
- (25) Casado, J. Para-Quinodimethanes: A Unified Review of the Quinoidal-Versus-Aromatic Competition and Its Implications. *Top. Curr. Chem.* **2017**, *375*, 73.
- (26) Rajca, A.; Wongsriratanakul, J.; Rajca, S. Magnetic Ordering in an Organic Polymer. *Science* **2001**, 294, 1503–1505.
- (27) Rajca, A. Organic Diradicals and Polyradicals: From Spin Coupling to Magnetism? *Chem. Rev.* **1994**, 94, 871–893.
- (28) Abe, M. Diradicals. Chem. Rev. 2013, 113, 7011-7088.
- (29) Joo, Y.; Huang, L.; Eedugurala, N.; London, A. E.; Kumar, A.; Wong, B. M.; Boudouris, B. W.; Azoulay, J. D. Thermoelectric Performance of an Open-Shell Donor—Acceptor Conjugated Polymer Doped with a Radical-Containing Small Molecule. *Macromolecules* **2018**, *51*, 3886—3894.
- (30) Vella, J. H.; Huang, L.; Eedugurala, N.; Mayer, K. S.; Ng, T. N.; Azoulay, J. D. Broadband Infrared Photodetection Using a Narrow Bandgap Conjugated Polymer. *Sci. Adv.* **2021**, *7*, No. eabg2418.
- (31) Coronado, E. Molecular Magnetism: From Chemical Design to Spin Control in Molecules, Materials and Devices. *Nat. Rev. Mater.* **2020**, *5*, 87–104.
- (32) Ponce Ortiz, R.; Casado, J.; Hernandez, V.; Lopez Navarrete, J. T.; Viruela, P. M.; Orti, E.; Takimiya, K.; Otsubo, T. On the Biradicaloid Nature of Long Quinoidal Oligothiophenes: Experimental Evidence Guided by Theoretical Studies. *Angew. Chem., Int. Ed.* **2007**, *46*, 9057–9061.
- (33) Mayer, K. S.; Adams, D. J.; Eedugurala, N.; Lockart, M. M.; Mahalingavelar, P.; Huang, L.; Galuska, L. A.; King, E. R.; Gu, X.; Bowman, M. K.; et al. Topology and Ground State Control in Open-Shell Donor-Acceptor Conjugated Polymers. *Cell Rep. Phys. Sci.* **2021**, 2, 100467.
- (34) Snyder, G. J. Rational Design of High-Spin Biradicaloids in the Isobenzofulvene and Isobenzoheptafulvene Series. *J. Phys. Chem. A* **2012**, *116*, 5272–5291.
- (35) Cullity, B. D.; Graham, C. D. Introduction to Magnetic Materials; Wiley: Hoboken, NJ, USA, 2008.
- (36) Becke, A. D. A New Mixing of Hartree–Fock and Local Density-Functional Theories. *J. Chem. Phys.* **1993**, 98, 1372–1377.
- (37) Frisch, M. J.; Trucks, G. W.; Schlegel, H. B.; Scuseria, G. E.; Robb, M. A.; Cheeseman, J. R.; Scalmani, G.; Barone, V.; Petersson, G. A.; Nakatsuji, H.; et al. *Gaussian 16*, Rev. C.01: Wallingford, CT, 2016.
- (38) Thakur, B.; Reddy, S. S.; Deshpande, U. P.; Amarendra, G.; Chakravarty, S. Evidence of Magnetism in RF Magnetron Sputtered

- Deposited Carbon Films and Investigation of Its Origin. *Carbon* **2019**, 154, 485–496.
- (39) Zeng, Z.; Liu, Y.; Zhang, W.; Chevva, H.; Wei, J. Improved Supercapacitor Performance of MnO₂-Electrospun Carbon Nanofibers Electrodes by Mt Magnetic Field. *J. Power Sources* **2017**, 358, 22–28.
- (40) Ieong, C.; Wang, Z.; Shi, W.; Wang, Y.; Wang, N.; Tang, Z.; Sheng, P.; Lortz, R. Observation of the Meissner State in Superconducting Arrays of 4-Å Carbon Nanotubes. *Phys. Rev. B: Condens. Matter Mater. Phys.* **2011**, 83, 184512.
- (41) Ney, A.; Kammermeier, T.; Ney, V.; Ollefs, K.; Ye, S. Limitations of Measuring Small Magnetic Signals of Samples Deposited on a Diamagnetic Substrate. *J. Magn. Magn. Mater.* **2008**, 320, 3341–3346.
- (42) Buchner, M.; Höfler, K.; Henne, B.; Ney, V.; Ney, A. Tutorial: Basic Principles, Limits of Detection, and Pitfalls of Highly Sensitive SQUID Magnetometry for Nanomagnetism and Spintronics. *J. Appl. Phys.* **2018**, *124*, 161101.
- (43) Sawicki, M.; Stefanowicz, W.; Ney, A. Sensitive SQUID Magnetometry for Studying Nanomagnetism. *Semicond. Sci. Technol.* **2011**, *26*, 064006.
- (44) MPMS3 Application Note 1500-023 Background Subtraction Using the MPMS3; Quantum Design, Inc.: San Diego, CA 92121 USA. 10307 Pacific Center Court, qdusa.com.
- (45) Dressler, J. J.; Cárdenas Valdivia, A.; Kishi, R.; Rudebusch, G. E.; Ventura, A. M.; Chastain, B. E.; Gómez-García, C. J.; Zakharov, L. N.; Nakano, M.; Casado, J.; et al. Diindenoanthracene Diradicaloids Enable Rational, Incremental Tuning of Their Singlet-Triplet Energy Gaps. Chem 2020, 6, 1353–1368.
- (46) Barker, J. E.; Dressler, J. J.; Cárdenas Valdivia, A.; Kishi, R.; Strand, E. T.; Zakharov, L. N.; MacMillan, S. N.; Gómez-García, C. J.; Nakano, M.; Casado, J.; et al. Molecule Isomerism Modulates the Diradical Properties of Stable Singlet Diradicaloids. *J. Am. Chem. Soc.* **2020**, *142*, 1548–1555.
- (47) Ji, X.; Leng, M.; Xie, H.; Wang, C.; Dunbar, K. R.; Zou, Y.; Fang, L. Extraordinary Electrochemical Stability and Extended Polaron Delocalization of Ladder-Type Polyaniline-Analogous Polymers. *Chem. Sci.* **2020**, *11*, 12737–12745.
- (48) Ji, X.; Xie, H.; Zhu, C.; Zou, Y.; Mu, A. U.; Al-Hashimi, M.; Dunbar, K. R.; Fang, L. Pauli Paramagnetism of Stable Analogues of Pernigraniline Salt Featuring Ladder-Type Constitution. *J. Am. Chem. Soc.* 2020, 142, 641–648.
- (49) Coak, M. J.; Liu, C.; Jarvis, D. M.; Park, S.; Cliffe, M. J.; Goddard, P. A. Squidlab A User-Friendly Program for Background Subtraction and Fitting of Magnetization Data. *Rev. Sci. Instrum.* **2020**, *91*, 023901.
- (50) Levenberg, K. A Method for the Solution of Certain Non-Linear Problems in Least Squares. Q. Appl. Math. 1944, 2, 164–168.
- (51) Marquardt, D. W. An Algorithm for Least-Squares Estimation of Nonlinear Parameters. J. Soc. Ind. Appl. Math. 1963, 11, 431–441.
- (52) Jesenik, M.; Beković, M.; Hamler, A.; Trlep, M. Analytical Modelling of a Magnetization Curve Obtained by the Measurements of Magnetic Materials' Properties Using Evolutionary Algorithms. *Appl. Soft Comput.* **2017**, *52*, 387–408.
- (53) Hansen, P. C. Rank-Deficient and Discrete Ill-Posed Problems; Society for Industrial and Applied Mathematics: Philadelphia, PA, USA, 1998.
- (54) Bain, G. A.; Berry, J. F. Diamagnetic Corrections and Pascal's Constants. J. Chem. Educ. 2008, 85, 532-536.
- (55) Dauben, H. J.; Wilson, J. D.; Laity, J. L. Diamagnetic Susceptibility Exaltation as a Criterion of Aromaticity. *J. Am. Chem. Soc.* 1968, 90, 811–813.
- (56) Krygowski, T. M.; Cyrański, M. K. Structural Aspects of Aromaticity. Chem. Rev. 2001, 101, 1385-1420.
- (57) Kahol, P. K.; Ho, J. C.; Chen, Y. Y.; Wang, C. R.; Neeleshwar, S.; Tsai, C. B.; Wessling, B. On Metallic Characteristics in Some Conducting Polymers. *Synth. Met.* **2005**, *151*, 65–72.

- (58) Boča, R. Temperature Dependence of Magnetic Susceptibility. In *Current Methods in Inorganic Chemistry*; Boča, R., Ed.; Elsevier, 1999; Chapter 6, Vol. 1, pp 315–344.
- (59) Bujak, P.; Kulszewicz-Bajer, I.; Zagorska, M.; Maurel, V.; Wielgus, I.; Pron, A. Polymers for Electronics and Spintronics. *Chem. Soc. Rev.* **2013**, *42*, 8895–8999.
- (60) Scheike, T.; Böhlmann, W.; Esquinazi, P.; Barzola-Quiquia, J.; Ballestar, A.; Setzer, A. Can Doping Graphite Trigger Room Temperature Superconductivity? Evidence for Granular High-Temperature Superconductivity in Water-Treated Graphite Powder. *Adv. Mater.* **2012**, *24*, 5826–5831.
- (61) MPMS3 Application Note 1500-021 Correcting for the Absolute Field Error Using the Pd Standard; Quantum Design, Inc.: San Diego, CA 92121 USA, 10307 Pacific Center Court. qdusa.com.
- (62) Magnetic Properties Measurement System MPMS3 User's Manual; Quantum Design, Inc.: San Diego, CA 92121 USA, 10307 Pacific Center Court. qdusa.com.
- (63) Landé, A. Über Den Anomalen Zeemaneffekt (Teil I). Z. Phys. 1921, 5, 231–241.